International Journal of Hydrogen Energy 95 (2024) 510–519

Contents lists available at ScienceDirect

International Journal of Hydrogen Energy

journal homepage: www.elsevier.com/locate/he

On the prospects of solid state hydrogen storage: First-principles investigations of two-Dimensional In_2CO

Hira Batool [a], Abdul Majid [a,*], Iram Shahzadi [a], Mohammad Alkhedher [b], Abdul Manan [c], Sajjad Haider [d], Kamran Alam [e]

[a] Department of Physics, University of Gujrat, Gujrat, 50700, Pakistan
[b] Mechanical and Industrial Engineering Department, Abu Dhabi University, Abu Dhabi, 59911, United Arab Emirates
[c] Department of Mathematics, Govt. Graduate College, Mandi Bahauddin 50400, Pakistan
[d] Chemical Engineering Department, College of Engineering, King Saud University, P.O.Box 800, Riyadh, 11421, Saudi Arabia
[e] VITO (Flemish Institute for Technological Research), Separation and Conversion Technology, Boeretang 200, 2400, Mol, Belgium

ARTICLE INFO

Handling Editor: Prof B Shabani

Keywords:
Hydrogen storage
In_2CO
Stability
Molecular dynamics
Adsorption
Desorption
Density functional Theory

ABSTRACT

The exploration of novel sources of hydrogen energy has been a prime research focus in recent past. Two-dimensional (2D) materials offering suitable physical and chemical qualities are considered advantageous for solid state hydrogen storage. In the present work, the novel 2D monolayer In_2CO is investigated for hydrogen storage using first-principles strategies. The thermodynamical, dynamical, and thermal stability of the material is studied using energetics, phonon modes and molecular dynamics calculations respectively. The structural and electronic properties of the material, along with the adsorption and desorption kinetics of H_2 molecules are systematically examined. The slab is found capable of binding thirty H_2 molecules at maximum with physisorption mode. The charge analysis of the monolayer with adsorbed H_2 molecules was also studied in order to explore the bonding and storage capacity of the material. The highest and average desorption temperatures are calculated as 300.4 K and 241.3 K respectively. The molecules may be effectively desorbed at 300 K, as per ab initio molecular dynamics (AIMD) simulations. The phenomenon of field desorption by applying electric field to fully loaded slab is also investigated. The findings of this work demonstrated the prospects of In_2CO slab for utilization as promising material for hydrogen storage applications.

1. Introduction

The rapid increase in energy demands owes to depleting conventional energy sources which triggered the search for sustainable, renewable, and environmentally friendly energy sources [1,2]. Hydrogen fuel is considered a promising sustainable option due to its abundant availability, renewable nature, cost-effectiveness, high energy density, and eco-friendly characteristics [2,3]. Currently, the practical usage of hydrogen energy is restricted due to a lack of effective storage materials, cost-effectiveness, and safety issues. The conventional methods of storing hydrogen include high-pressure gas or low-temperature liquid but these modes are insecure and costly for wide commercial utilization [4]. The issues related to conventional gaseous and liquid hydrogen storage methods cannot be suitably addressed when future requirements are taken into account. Thus, it is essential to explore the methods of solid-state hydrogen storage which offer high efficiency, have high storage density, easy transportation, and cost-effectiveness.

The United States Department of Energy set 2025 as a goal year to create systems capable of storing hydrogen with a 5.5 wt percentage with a temperature range of 233–358 K [3,5,6]. In this regard, the increasing spectrum of lightweight 2D materials with suitable properties is giving hope to meet the objectives related to hydrogen storage. The elemental 2D materials comprising boron, carbon, nitrogen atoms, and several compounds have been found appropriate for hydrogen storage. There has been a variety of chemically, dynamically, and thermally stable materials that are lightweight, pore structured, and offer large specific surface areas for storing hydrogen molecules [7–9]. However, the pristine nanomaterials are often found to have poor hydrogen storage capacity under normal conditions due to unfavorable H_2 molecular adsorption energy with values less than −0.1 eV/H_2 [8–10]. The optimal H_2 adsorption energy for practical usage should fall within 0.1–0.6

* Corresponding author.
E-mail address: abdulmajid40@yahoo.com (A. Majid).

https://doi.org/10.1016/j.ijhydene.2024.11.264
Received 28 July 2024; Received in revised form 14 November 2024; Accepted 15 November 2024
Available online 20 November 2024

eV/H_2 to guarantee reversible adsorption and desorption mechanism [11,12]. Moreover, the adsorption strength must fall within the irreversible energy range, and the energy must be greater than 0.1 eV/H_2 for efficient adsorption and advantageous kinetic characteristics [13,14].

The most efficient approach to storing H_2 is considered chemisorption and physical adsorption of the molecules on the surface of the solid-state substance. Metal-organic structures, carbon nanotubes, and zeolites show high efficacy in physical adsorption of hydrogen [12,15]. Because of reversible functioning at lower temperatures and moderate pressures, the absence of chemical bonds, and the high degree of interaction between the adsorbent and the adsorbate, the physisorption of H_2 is a potential solid-state hydrogen storage mechanism [16]. By using Dewar coordination to decorate the 2D monolayer with transition metals (such as V, Ti, and Ni), alkali metals (Li, Na, and K), and alkaline earth metals (Be and Ca), one can enhance the performance of pure 2D materials [17]. The expected outcome is the formation of bonds by Kubas or electrostatic contacts between the adsorbed hydrogen molecules [18,19].

The metals owing to huge bulk cohesive energy may appear in the form of agglomerating atoms on the surface during the decoration process which decreases H_2 storage efficiency in practical applications. Despite possessing a strong metal-H_2 interaction, integrating massive transition metals also causes the pristine material to become heavier, which lowers hydrogen storage capacity. Hence, the electric field is also applied that causes charge polarization is another method to increase the material's performance even though it makes the process expensive [20,21]. The available literature points out that it is not easy to find pure, affordable, stable, metal-free material that can hold hydrogen reversibly at room temperature.

The 2D materials related to p-block elements offer advantages of chemical and mechanical stability in addition to their cost-effectiveness and lightweight character. The synthesis of materials comprising atoms with comparable atomic sizes, such as carbon, boron, and nitrogen, may be considered to further increase the storage efficiency [22–25]. The charges have been found redistributed on the surface of $B_xC_yN_z$ due to differences in electronegativity between the constituent atoms [26,27]. The adsorption energy can be increased if polarization-dependent interactions are increased. The realization of 2D $B_xC_yN_z$ materials with a uniform and even distribution of B, C, and N has significantly increased as per theoretical and experimental investigations 28–30. This work is aimed at exploring the prospects of In_2CO for hydrogen storage application, using first principles methods based on DFT and AIMD simulations. In_2CO is a novel 2D material computationally designed by combining In-doped and O-doped graphene layers [31]. In_2CO's unusual structure promotes strong covalent bonding between In, C, and O atoms creating a stable quasi-planar material. The incorporation of In into graphene creates a unique electronic structure, making In_2CO appropriate for application in hydrogen storage and energy conversion. The material's stability stems from balanced interactions between In, C, and O atoms which form a mixed bonding network that not only increases its robustness but also provides suitable electronic properties. In_2CO is believed to have tremendous potential in the realm of 2D materials. While this compound has yet to be synthesized, it is expected to cause an advancement in the creation of useful 2D materials. The findings of this study shed light on suitability of In_2CO for efficient hydrogen storage technology.

2. Computational detail

This work is carried out using the first-principles methodology employed in the Amsterdam density functional (ADF) package for the investigation of In_2CO slabs to store hydrogen [31]. ADF employs a linear combination of atomic orbitals (LCAO) approach using Slater orbitals to describe the atomic orbitals for precise prediction on structures and energy calculations. The geometry of the structures was optimized by using triple-zeta polarization (TZP) basis sets which are known to accurately describe the electronic density of oxides [32]. ADF offers frozen core approximation in the form of large, medium, small, and none. The calculations were performed using the 'none' option to ensure all-electron calculations ensure the accuracy of adsorption energies. The electron interactions were implemented using exchange-correlation GGA-PBE (generalized gradient approximation, Perdew-Burke-Ernzerhof) [33]. Further, to include the van der Waals interactions between the molecules and the slabs, the Grimme D3 dispersion correction was also added [34].

The convergence criteria for the gradient was 0.001 eV/Å, the step convergence value was 0.01 Å and the energy convergence was 10^{-6} eV. The dynamic and thermal stability of the material was studied with the help of phonon dispersion curves and Ab initio molecular dynamics (AIMD) respectively [35]. For the thermal stability analysis of pristine material and adsorbed H_2, the calculations were performed using a thermostat Nose-Hoover chain. The method employs a canonical ensemble between the actual system and the heat bath by exchanging the fabricated energy. The energy-transferring is controlled by Q (imaginary mass) which provides the high-frequency oscillations to the system coupled with heat bath and low-frequency oscillations to the actual/real system [36].

The hydrogen storage capacity or the storage density $C_{wt\%}$ is calculated by the formula given in equation (1).

$$C_{wt\%} = \frac{n \times M(H_2)}{n \times M(H_2) + M(In_2CO)} \tag{1}$$

Where M(H_2) and M(In_2CO) are the molar mass of a single hydrogen molecule and In_2CO slab and n represents the adsorbed hydrogen molecules on the host structure [31,37–39]. For the highest capacity of the hydrogenated systems, the desorption temperature is computed with the help of the Van't Hoff formula given in equation (2).

$$T_D = \frac{E_{ads}}{k_B}\left(\frac{\Delta S}{R} - \ln p\right)^{-1} \tag{2}$$

Where k_B and R are the Boltzmann and gas constants respectively, ΔS represents the entropy change for the transition of hydrogen gas into liquid phase which is 75.44 $Jmol^{-1}K^{-1}$, p is the pressure at equilibrium state which is 1 atm and the E_{ads} is the energy of adsorption for highest hydrogenated capacity [40,41].

The energy of the formation of the structures is calculated using equation (3) thereby ensuring the exothermic conditions.

$$E_{form} = \frac{E_{In2CO} - xE_{In} - yE_C - zE_O}{x + y + z} \tag{3}$$

Where E_{In_2CO} is the energy of the slab, E_{In}, $E_{C,}$ and E_O are the atomic energies of indium, carbon, and oxygen atoms further, $x, y\ z$ are number of atoms in the reaction [42].

The value of the adsorption energy of H_2 molecules on the surface of the In_2CO slab is calculated using the formula given in equation (4).

$$E_{ad.H_2} = \frac{E_{total} - E_{In_2\ CO} - nE_{H_2}}{n} \tag{4}$$

Where E_{Total}, E_{In_2CO}, and E_{H_2} are energy values of the H_2 adsorbed surface, In_2CO, and H_2 molecule respectively, whereas n denotes the H_2 molecules adsorbed on the surface [43].

3. Results and discussion

The structural properties, electronic properties, and thermal, dynamical, and thermodynamical stability of In_2CO were comprehensively investigated. Further, the optical and thermodynamical properties of the material have been reported elsewhere out of which few findings are described here for the sake of completeness [31]. The adsorption behavior of H_2 molecules over the monolayer was explored to find out its

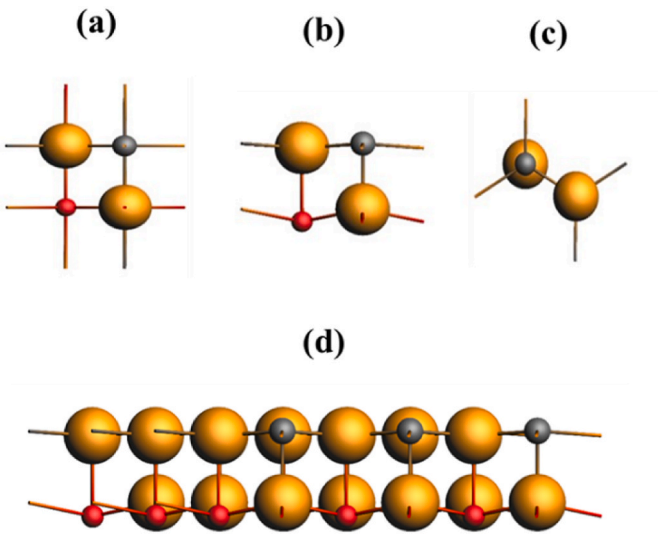

Figure-01. The optimized structure of In_2CO (a) Unit cell consisting of 4 atoms (b), (c) The slab along the x-axis and z-axis view (c) The side view of a supercell of 3 × 3 slab. The orange, gray, and red colors represent indium, carbon, and oxygen respectively.

adsorption energy E_{ads}, $C_{wt\%}$, and desorption temperature. The AIMD simulation was performed for information about the hydrogen adsorption and release at different temperatures. The findings of the study are described in the following sections.

3.1. Structural properties

The bulk In_2CO has a hexagonal crystal structure with $\overline{P}$ 6m2 space group [31]. There are two inequivalent In locations in the structural arrangement of the material. In the first location, In^{3+} is attached with two corresponding C^{4-} and three equivalent O^{2-} atoms to form trigonal bipyramids InC_2O_3 which shares corners with eight equivalent InC_2O_3 trigonal bipyramids, and boundaries with six equivalent InC_3O_2 trigonal bipyramids. In the second location, In^{3+} is attached with three equal C^{4-} and two equivalent O^{2-} atoms to form InC_3O_2 trigonal bipyramids that share corners with eight equivalent InC_3O_2 trigonal bipyramids and boundaries with six equal InC_2O_3 trigonal bipyramids. C^{4-} is bonded to five In^{3+} atoms to form CIn_5 trigonal bipyramids that link the corners with eight equivalent CIn_5 trigonal bipyramids and edges with six equivalent OIn_5 trigonal bipyramids. O^{2-} is bonded to five In^{3+} atoms to form OIn_5 trigonal bipyramids that share corners with eight corresponding OIn_5 trigonal bipyramids and edges with six equivalent CIn_5 trigonal bipyramids. The optimized structure of In_2CO slab unit cell and monolayer along different directions are shown in Fig. 1. The calculated lattice constants for In_2CO were found to be a = 3.90 Å, b = 3.90 Å, and c = 4.76 Å whereas $\alpha = \beta = 90^\circ$ and $\gamma = 120^\circ$. The volume of the unit cell is 63.5 Å. The results revealed that both In–C bond lengths are 2.25 Å and both In–O bond lengths are 2.25 Å. The interatomic distance of In–C is 2.38 Å and for In–O is 2.38 Å.

The relaxed structure of the In_2CO slab is given in Fig. 1 (b) and (c) for the unit cell. The structure comprised of 2 In atoms and 1 C and 1 O atom. The augmented lattice constants are a = b = 3.90 Å and $\alpha = \beta = \gamma = 129^\circ$. The unit cell area was 13.3 $Å^2$. The interatomic distances are In–C (2.27 Å), In–C (2.19 Å), In–O (2.30 Å), and In–O (2.47 Å), The shortest interatomic distances between In–C and In–O are 2.19 Å and 2.30 Å that are regarded as bond lengths. The side view of the 3 × 3 supercell employed for the application of the material for hydrogen adsorption is shown in Fig. 1 (c).

3.2. Stability analysis

3.2.1. Thermodynamical stability

To analyze the thermodynamical stability of In_2CO, its formation energy was calculated using equation (3) which yielded a value of −1.399 eV that points to an energetically stable structure. In addition to the LCAO approach, the formation energy was also calculated by the plane wave approach that is implemented in the Vienna Ab initio Simulation Package (VASP) which yielded a value of −0.647 eV. The findings indicate that the reaction in the formation of the structure is exothermic thus pointing to an energetically stable structure of In_2CO.

3.2.2. Dynamic stability

The phonon spectra were calculated by taking a 3 × 3 × 3 supercell of In_2CO containing 108 atoms. The phonon spectra indicate the absence of negative modes that ensure the dynamic and kinetic stability of the material. The phonon band structure calculated along high symmetry

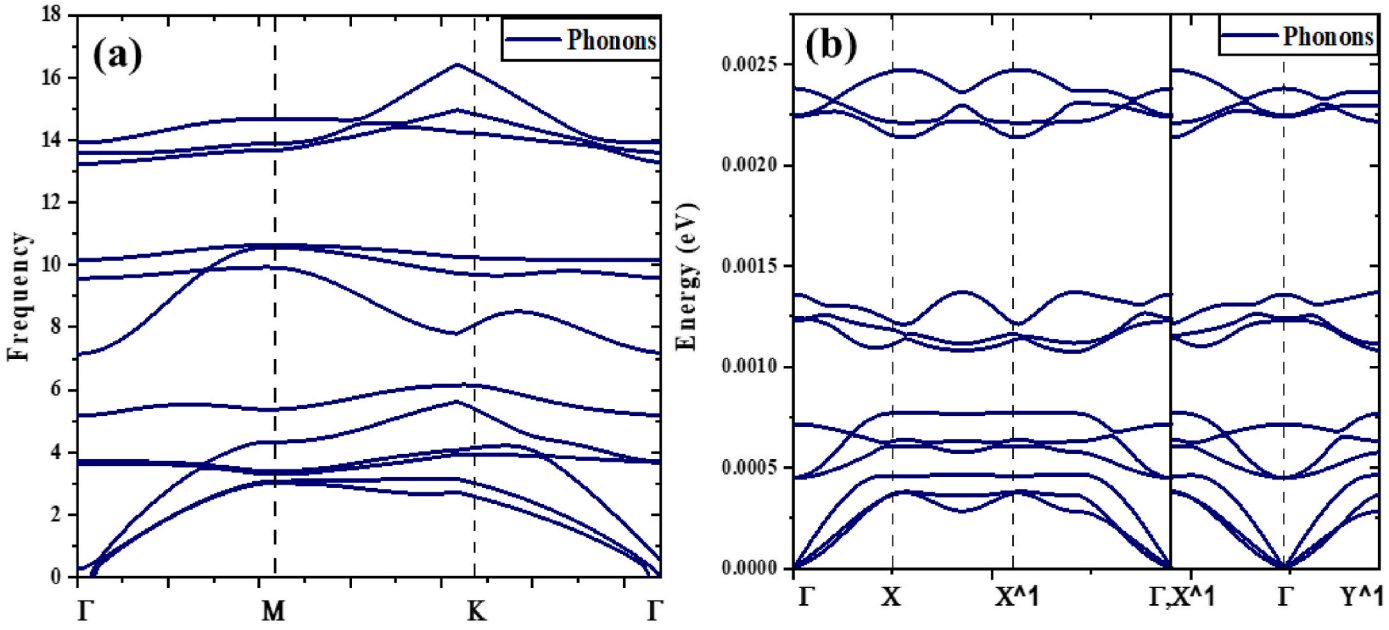

Figure-02. The calculated phonon dispersion curves for (a) bulk In_2CO (b) slab In_2CO.

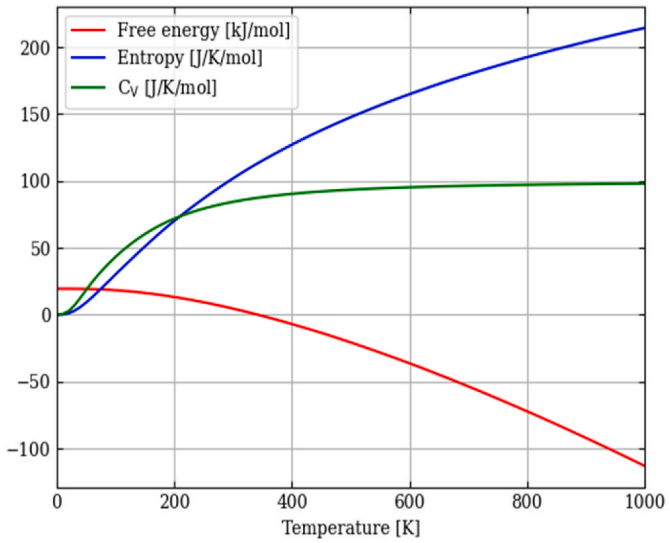

Figure-03. The calculated temperature-dependent behavior showing entropy, enthalpy, and free energy of the In_2CO slab.

points is illustrated in Fig. 2 (a). The *in-plane* longitudinal-acoustic (LA) and transverse-acoustic (TA) modes are higher in energy than the *out-of-plane* acoustic (ZA) modes. Though the results exhibit that the situation near the Gamma-point is analogous to that of graphene, we will concentrate on the three acoustic modes. The acoustic modes with high dispersion values are responsible for thermal transport properties in most of the solid materials.

Similarly, the phonon band structure for In_2CO slab is shown in Fig. 2 (b). The absence of negative frequencies in the phonon graph ensures the dynamic stability of the structure. Fig. 3 illustrates how enthalpy, free energy, entropy and heat capacity change with temperature. The graph shows that the free energy declines with temperature, entropy, heat capacity and enthalpy all rise as temperature rises. We observed that the In_2CO intermetallic heat capacity increases exponentially than the enthalpy and entropy, indicating that the In_2CO heat capacity is more temperature sensitive than entropy and enthalpy. At room temperature entropy, enthalpy, and free energy are predicted to be 0.081 eV, 0.465 eV, and 0.069 eV respectively. At low temperatures, the phonon contribution dominates whereas at high temperatures, the electronic character plays leading role. The heat capacity at constant volume (C_v) grows steadily with temperature, and eventually approaches a constant value 172.836 cal/mol K, as the Dulong Petit limit [44]. For In_2CO, C_v is calculated as 166.813 cal/mol K under ambient conditions.

3.2.3. *Thermal stability*

The AIMD simulation is a very resourceful strategy to examine the thermal stability of materials [45,46]. The 3x3 supercell of the material was used in the simulations in which the calculation continued for 500 steps with a time-step of 0.25 fs which was adequate to estimate the thermal stability of the material. The plots of temperature vs time step and energy vs the time steps are given in Fig. 4 along with the snapshots obtained at the beginning and after different time steps the final structure after 10 ps. The energy fluctuates around the mean position retaining the stability of the structure. After the simulation, the structure of the In_2CO slab remains intact at 300 K which indicates the thermal stability of the material at room temperature.

3.3. *Electronic properties of In_2CO*

The electronic properties of In_2CO were investigated on the basis of single point calculations of electronic band structure and density of states (DOS) [47]. The material exhibited metallic nature as per band structure provided in Fig. 5 (a). The total and partial DOS chart of the material is shown in Fig. 5 (b) according to which In-s and In-p orbitals show major contribution in the states around Fermi level. The C-p orbitals from −2 to 2.5 eV exhibit higher states when compared with In-p states. It has been known that narrow bandgap semiconductors or metallic materials exhibit potential for hydrogen storage [48,49]. The electronic properties and carbonaceous character of the material points to its suitability for H_2 adsorption and storage. The electronic properties of the material after adsorption of H_2, will be described in the coming sections in order to understand the impact of hydrogen on the adsorbent's electronic character.

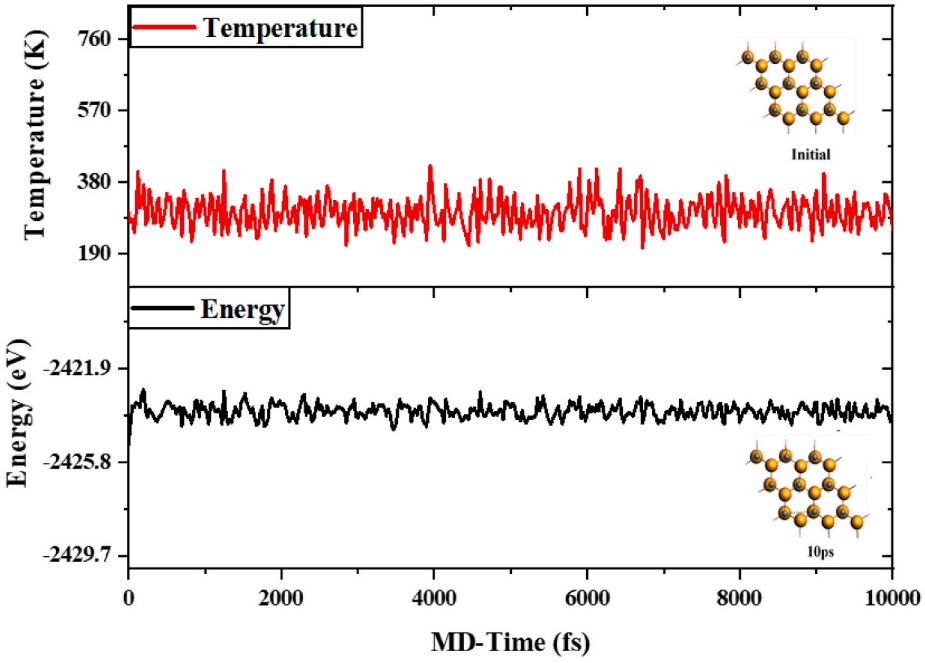

Figure-04. The temperature variation and change in free energy of the In_2CO slab supercell as a function of time as determined by MD simulations.

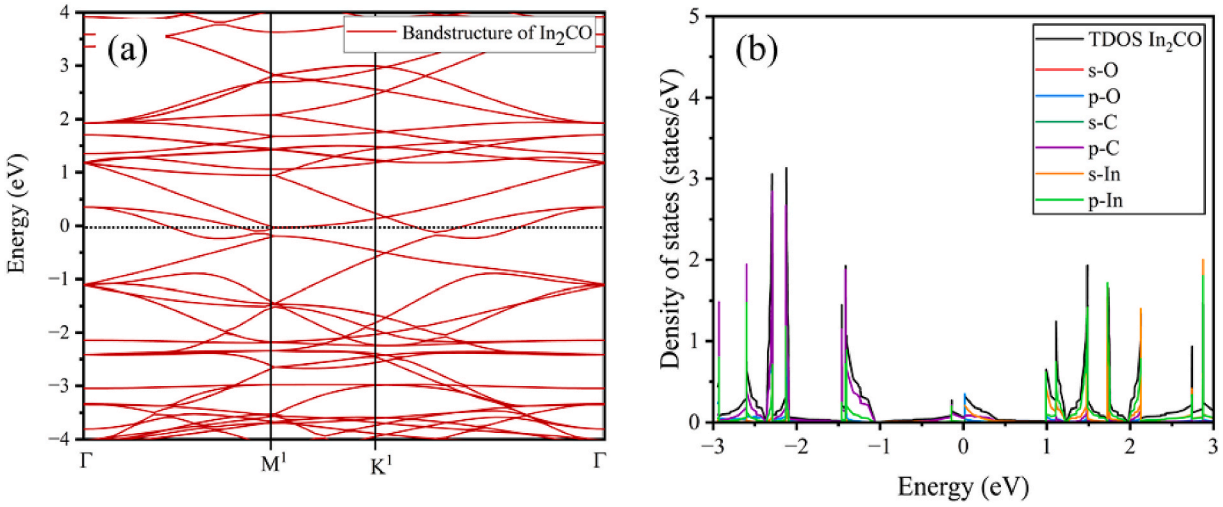

Figure-05. The electronic properties of 3 × 3 slab of In_2CO (a) Band structure diagram (b) Partial density of states (PDOS) and total density of states (TDOS) of In_2CO. Fermi level is set to 0 eV.

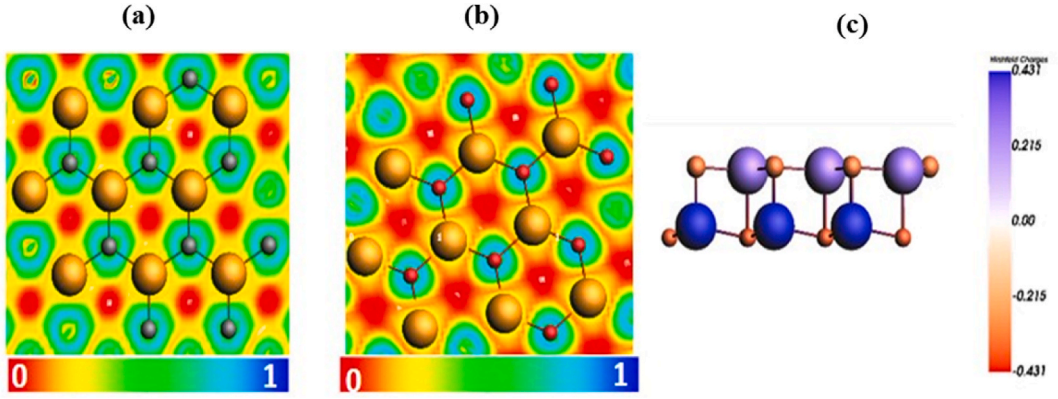

Figure-06. Electron Localization Function plot of In_2CO (a) viewed from the top (b) viewed from the bottom (c) Hirshfeld charge analysis.

3.4. Charge analysis

Hirshfeld-charge analysis is carried out to investigate the charge transfer between atoms of the structure as shown in Fig. 6 (c)[31]. The values of electronic charge appeared on atoms as In (1) as 0.470 e, In (2) as 0.279 e, whereas on C as −0.452 e and O as −0.314 e. The total values of Hirshfeld charges are In (0.749 e), C (−0.452 e), O (−0.314 e). The charge analysis indicated that In is positively charged while C and O are negatively charged which points to the fact that electronic charge is transferred from In to C and O during the process of bond formation. Hirshfeld charge analysis confirmed that In (1), is more positive and the charge is transferred from the indium atom to carbon atoms that is more negative than oxygen atoms. Whereas In (2), is less positive and they are the on the other side of the hexagon and it has transferred charge to O atoms. The Hirshfeld charge values for In and C suggest that they will form a polar covalent bond. The analysis indicates a partial positive charge on In and a partial negative charge on C. This suggests that electrons are shared between the In and C atoms, resulting in a polar covalent bond [50]. The difference between the Hirshfeld charge values suggests that the bond is partially ionic. This indicates that the electrons are distributed unequally between two atoms, with the C atom holding a larger share of the electron density because of its higher electronegativity [51]. These findings suggest that electrons are transported from the O to the In atom, which results in the formation of ions with opposite charges.

The difference in magnitude of Hirshfeld charges between two atoms is 0.593 e which suggests that the bond is relatively covalent [52]. This indicates that there is a substantial transfer of electrons from O to In, subsequent in the development of In^{3+} and O^{2-} ions. Overall, the Hirshfeld charge values for O to In suggest the formation of a covalent bond [53].

The electron-localization-function (ELF) is a supportive method to study how electrons delocalize in solids which provides bonding information [54]. When the result is renormalized to a value between 0 and 1, the ELF shows the structure of the atomic shells [55]. The ELF for In_2CO slab along different planes is shown in Fig. 6(a) and (b). The yellow color appears around In atoms in Fig. 6(b) which represents electron delocalization or deficiency of charge there. The ELF value 0.5 indicates that there is an ionic bond between C and In as well as In and O atoms but there is the possibility of a slighter covalent character. It is because the ELF value is closer to 0.5 indicating that both electron transfer and covalent electron sharing are happening in considerable amounts at the same time. The electronegativity difference between C and In is 0.8 and for In and O, its value is 1.8 calculated from the Pauling scale of electronegativity also supports the fact that bonding between In–O and In–C will be ionic with slight covalent character [31,56].

The covalent radii of In, C, and O are 1.42 Å, 0.76 Å, and 0.66 Å respectively according to which the sum of the covalent radii of In–C is 2.18 Å and In–O is 2.08 Å [57]. Similarly, the ionic radii of In, C, and O are 0.94 Å, 0.30 Å, and 1.26 Å respectively and the sum of the Ionic radii of In–C is 1.24 Å and that of In–O is 2.20 Å [58]. The calculated values of bond lengths of In–C and In–O are 2.25 Å and 2.25 Å respectively. The

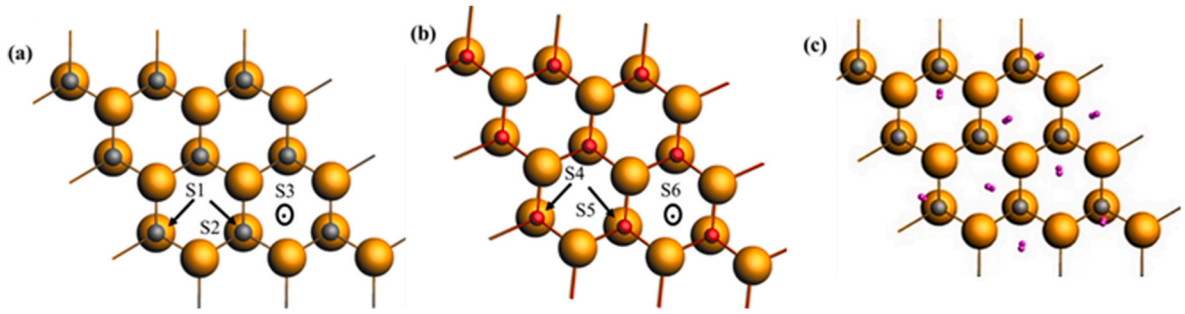

Figure-07. The adsorption sites named as S1, S2, S3, S4, S5, and S6 situated on the monolayer In_2CO with (a) top view (b) bottom view, and (c) the optimized H_2 molecule adsorption near the most suitable site on In_2CO surface viewed from the top.

Table-01
Different adsorption sites along with the calculated energy values.

Adsorption site	E_{ads} (eV)	Adsorption site	E_{ads} (eV)
S1	−0.245	**S4**	−0.201
S2	−0.441	**S5**	−0.138
S3	−0.025	**S6**	−0.071

Table-02
The calculated distances between the adsorbed molecules and surface and average adsorption-energy of H_2.

Number of H_2 Molecules	Adsorption Energy E_{Ads} (eV)	H_2-surface distance (Å)	d_{H-H} (Å)
In_2CO–H_2	−0.2261	2.80	0.77
In_2CO-$(H_2)_4$	−0.2349	2.44	0.77
In_2CO-$(H_2)_8$	−0.2135	2.49	0.77
In_2CO-$(H_2)_{12}$	−0.1859	2.76	0.77
In_2CO-$(H_2)_{16}$	−0.1573	2.50	0.77
In_2CO-$(H_2)_{20}$	−0.1514	2.54	0.77
In_2CO-$(H_2)_{24}$	−0.1456	2.92	0.77
In_2CO-$(H_2)_{28}$	−0.1480	2.76	0.77
In_2CO-$(H_2)_{30}$	−0.1229	2.63	0.77

sum of covalent radii and ionic radii is less than the computed bond lengths, which means the bonding nature is specifically ionic or might be polar covalent slightly.

3.5. Hydrogen adsorption on In_2CO slab

To examine the efficiency of In_2CO for hydrogen storage, the performance of H_2 molecules adsorbed on the surface of the material was thoroughly investigated. The suitable adsorption site was determined by conducting energy profiling of the adsorption on different available sites of the surface. The calculations carried out for six high symmetry sites are depicted in Fig. 7 (a) and (b) and the relevant adsorption energies are given in Table 1. The employed sites are chosen as S1 lies above the carbon atom, S2 is situated above the In atom, and the hollow site is present at the center of ring InC is denoted by S3. Similarly, for ring InO, the hollow site is named S6, the site located above the oxygen atom is S4, and the site positioned above the In atom is named S5. The mechanism is investigated by studying how hydrogen molecules interact with the material on the atomic level. Hydrogen molecules are adsorbed one by one onto the surface of the host structure. The calculated values of the adsorption energies are found in the range from −0.025 to −0.441 eV. The analysis indicates that, among all the possible sites H_2 molecules energetically prefer to occupy the hollow site locations close to carbon atoms. This finding is also confirmed by the adsorption energy of S3 and S6, for which the H_2 molecules exhibit a vertical distance of 2.72 Å from the carbon atoms and 3.33 Å from the other molecules. Fig. 7 (c) displays the final optimized configurations with the complete relaxation of H_2 molecules. The average length of the d_{H-H} bond should be approximately 0.77 Å, which is greater than the typical length of the H_2 molecule having a value of 0.74 Å [59].

The value of the adsorption energy of H_2 molecules on the surface of

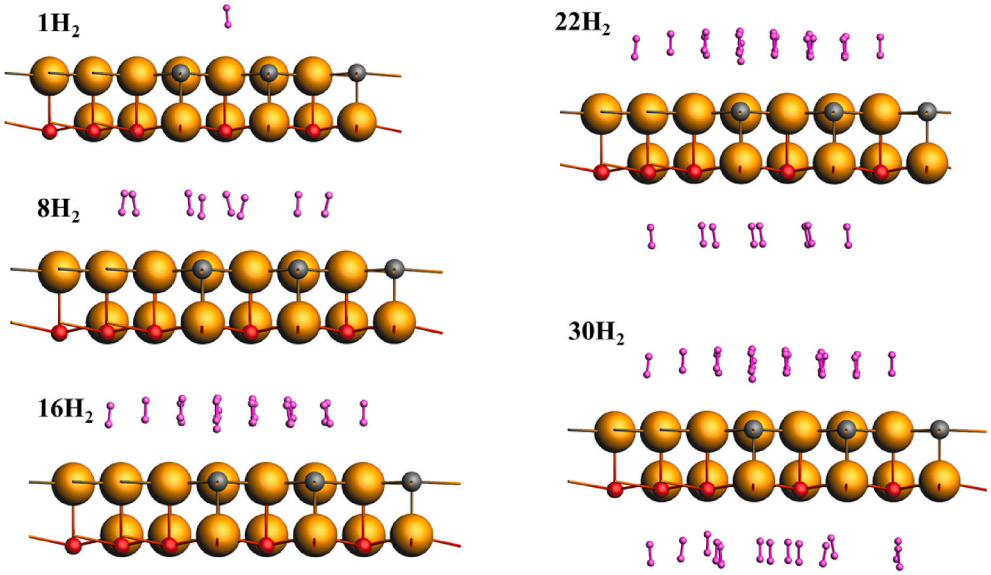

Figure-08. The optimized monolayer of H_2 molecule adsorbed In_2CO is shown for a few adsorption cases from 1 to 30.

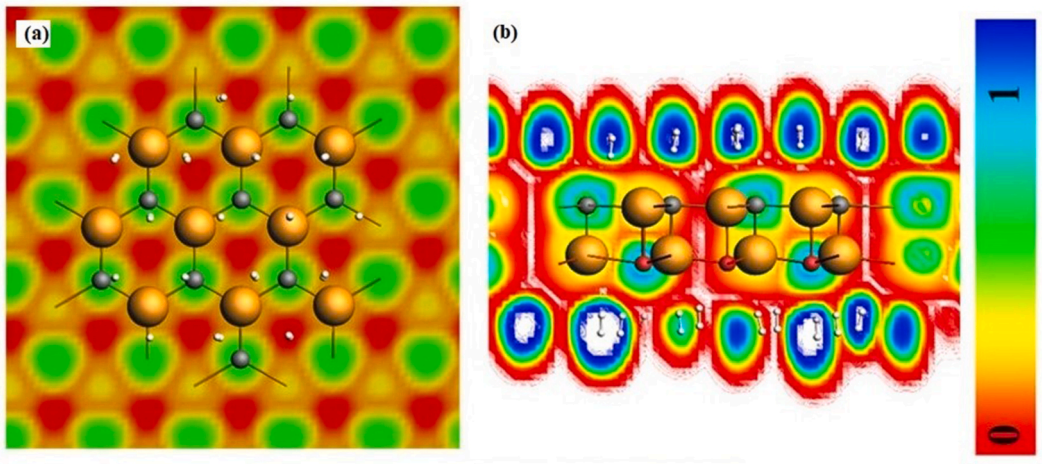

Figure-09. Electron Localization Function (ELF) Plot of H_2 molecules adsorbed In_2CO slab with (a) top view (b) side view.

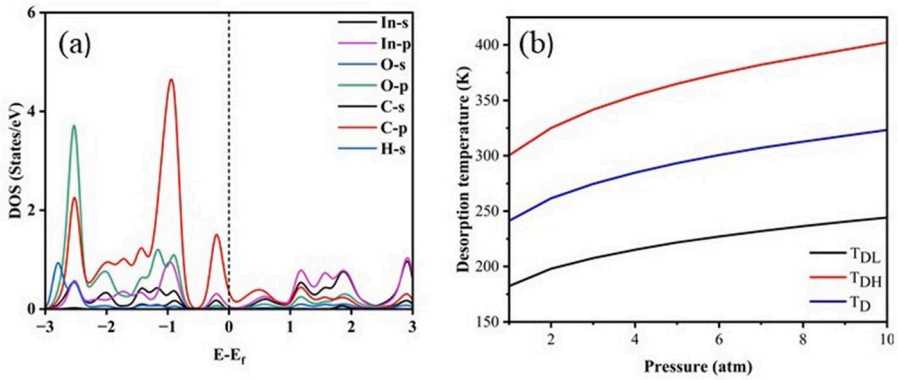

Figure-10. (a) The PDOS calculated for H_2 adsorbed In_2CO monolayer for *E*-E_f. (b) The relationship of desorption temperature for equilibrium pressure up to 10 atm.

In_2CO was calculated using equation (4) [60,61]. Table 2 summarizes the regular adsorption energy of H_2 by gradually increasing the number of adsorbed molecules.

The values of adsorption energies range from −0.234 eV to −0.145 eV found within the optimal adsorption energy range of −0.2 to −0.7 eV/H_2 which lies between the physisorbed and chemisorbed cases [62, 63]. The negative adsorption energy symbolizes the spontaneous process of adsorption on the surface of the material. The system was allowed to fully optimize after increasing the number of adsorbed H_2 molecules until further adsorption on the host surface became unfeasible due to repulsion from the slab. It appeared that the active system became unable to allow further adsorption of more than 30 hydrogen molecules. The distance of the H_2 from the different atoms of In_2CO ranges from 2.44 Å to 2.92 Å while the distance of hydrogen atoms to each other remains the same at 0.77 Å throughout. Fig. 8 shows the absorbed H_2 molecules starting from one molecule and reaching the maximum capacity of $(H_2)_{30}$. The entire H_2 molecules are well distributed over the whole monolayer without disturbing its stability and structure.

The adsorption percentage is calculated by formula (1), and the storage capacity $C_{wt\%}$ is found as 2.54 % for the highest hydrogenated system. The well-known tin carbide monolayer along with TM atoms (transition metals) also exhibits hydrogen storage capacity ranging up to 5% [64].

3.5.1. *Charge analysis of H_2 adsorbed In_2CO*

The ELF plots H_2 adsorbed In_2CO are given in Fig. 9 for a qualitative understanding of changes in charge transfer characteristics. The attractive interactions of H_2 with the In_2CO surface are produced by the occurrence of charge transfer from an indium atom in the direction of the H_2 molecules. The charge transfers from In_2CO towards hydrogen molecules in_2CO-nH_2 complexes decrease as the number of H_2 molecules increases. The hydrogen with high charge density represents the perfectly localized electrons while the indium represents the delocalization of charge there. The bond between electropositive and electronegative is polar and tends to become ionic.

3.5.2. *Electronic properties after H_2 adsorption*

The storage capacity of hydrogen can be understood by analyzing the electronic DOS of the adsorbed slab. The calculated DOS after the H_2 adsorption on In_2CO is shown in Fig. 10.

The electronic character of the slab remains metallic after the hydrogen adsorption. The total DOS remains the same after increasing the number of H_2 molecules and the contribution of H-s orbitals is comparable to C-s orbitals. The analysis points to moderate interaction between the host and the molecules as the hybridization between the green-colored *O*-p orbitals and pink-colored In-p is observed. The mechanism of hydrogen storage is usually studied via binding between the adsorbate and the adsorbent. The H-s orbital shows significant peaks near the Fermi level, which strongly indicates that hydrogen interacts with the In₂CO surface. Additionally, the In-p orbital (depicted in purple) overlaps with these peaks, suggesting a clear interaction through hybridization with the H-s orbital. Notably, the prominent peaks around −1 eV suggest strong hybridization between the H-s and In-p orbitals, which plays a key role in stabilizing hydrogen atoms on the In₂CO surface as an essential aspect for effective hydrogen storage. This covalent bonding, along with van der Waals forces (evident from the overlap and

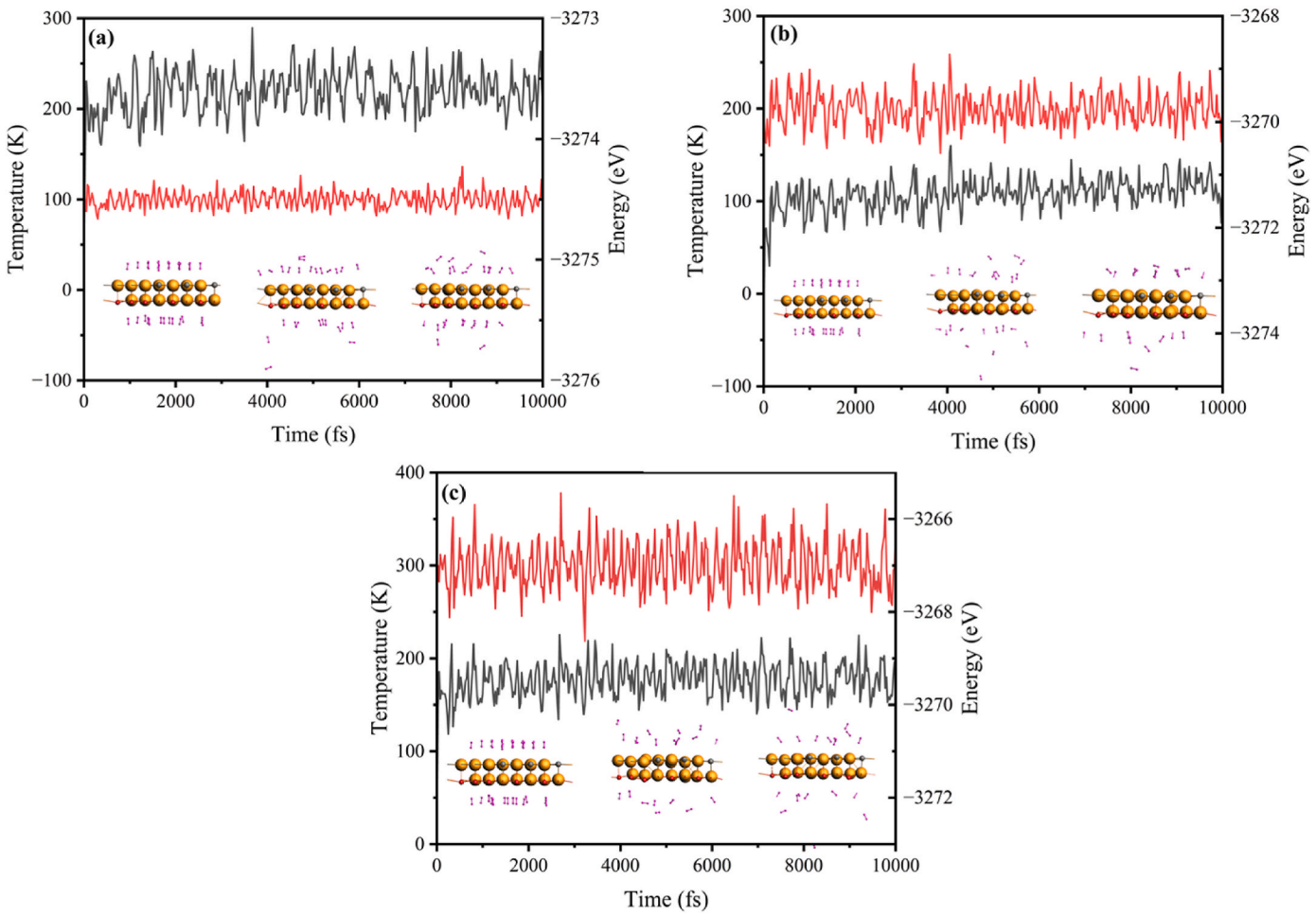

Figure- 11. AMID simulation of the In_2CO-$(H_2)_{30}$ at different temperatures for the comparison to study the H_2 release.

intensity of the DOS peaks near the Fermi level), supports a robust chemisorption mechanism.

3.5.3. *Desorption and Hydrogen Release Dynamics*

The release or desorption of already adsorbed hydrogen molecules from the slab is essentially required. We investigated the prospects of desorption of hydrogen molecules via the application of thermal energy as well as the electric field as elaborated in the following.

3.5.3.1. Thermal desorption. To estimate the desorption performance of a hydrogen-storing material, the calculation of desorption temperature is useful as it helps to define the merit of the material at ambient conditions. Using equation (2) the desorption temperature is calculated as the lowest desorption temperature T_{DL}, highest desorption temperature $T_{DH,}$ and the average T_D. The T_{DH} is calculated as 300.40 K which indicates the release of the stored hydrogen near-ambient conditions. Hence, it is the maximum temperature required to release the pre-adsorbed hydrogen from the slab. The minimum temperature which is required to initiate the process of hydrogen release is calculated as 182.36 K. The graph between the T_D at different equilibrium pressures is also explained for better understanding as shown in Fig. 10 (b). The red line shows the highest desorption temperature, the black line shows the lowest, and the blue line shows the average desorption temperatures. The desorption temperatures are in good agreement with the relevant reported values in the literature [37,40].

The hydrogen release dynamics are investigated at different temperatures by conducting AMID simulations for the fully loaded system In_2CO-$(H_2)_{30}$. Three AMID simulations were performed at different temperatures 100 K, 200 K, and 300 K with a time step of 10,000 fs as shown in Fig. 11. The comparison of the energy oscillations with respective temperatures can be seen in Fig. 11 (a), (b), and (c) according to which the significantly higher oscillations of energy are observed at 300 K rather than 100 K. The results showed that the changes in structure may be presented at 300 K. The observation of the bond length variations of In–H is helpful in understanding the H_2 release from the slab. The bond lengths for only five In–H bonds are found larger than 5 Å at 100 K, which shows that the five H_2 molecules will run away from the host. The number of H_2 molecules departing away from the surface increases up to eight when the temperature arrives at 200 K as shown in Fig. 11(b). When the temperature of the simulation increases to 300 K, the desorption leads large number of H_2 molecules that escape from the surface having bond lengths greater than 5 Å. The simulations point to an efficient release of pre-adsorbed H_2 molecules at desorption temperature.

3.5.3.2. Field desorption. To further investigate the desorption behavior of hydrogen molecules from the slab, the slab was placed in an external electric field applied perpendicular to it [65,66]. The findings based on the calculations revealed that we can desorb a sizable number of hydrogen atoms from the In_2CO surface in a temperature range that is appropriate for fuel cell applications. Consequently, this offers a handy method for releasing the adsorbed molecules from the surface of In_2CO. The values of the electric field were raised to 10 V/Å in incremental steps of 2 V/Å and structural relaxations were carried out at every value of the applied field. When a field is applied perpendicular to the direction of the slab, no notable structural deformation takes place. The

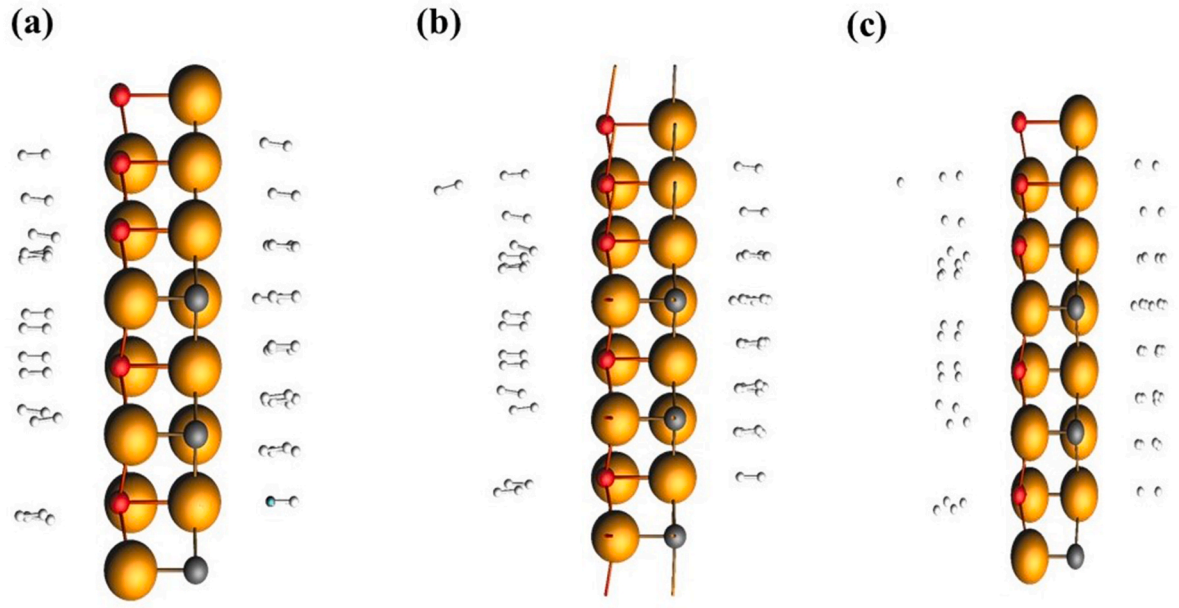

Figure-12. Structure of In_2CO-$(H_2)_{30}$ at different applied Electric fields (a) at 2 V/Å (b) 8 V/Å and (c) at 10 V/Å.

applied electric field weakened the bond between hydrogen and surface atoms, as a result, the distance between hydrogen molecules kept on increasing with the increase of the applied external electric field, and at 10 V/Å all the hydrogen molecules were successfully desorbed from the surface as shown in Fig. 12. The H_2 to host surface distance was increased from 2.47 Å to 2.57 Å at 2 V/Å. The distance was increased up to 2.69 Å when an electric field was switched on with value 4 V/Å whereas in the case of the field 4 V/Å the distance was increased up to 3.82 Å. With further increase the field to 8 V/Å the distance was increased up to 4.99 Å for the molecules adsorbed on the bottom side of the layer. It was also observed that the molecules adsorbed to the bottom side of the layer tend to desorb faster than those present at the upper side of the layer due to weak adsorption between hydrogen and oxygen atoms. At 10 V/Å the average distance was increased up to 5.99 Å confirming the complete desorption of H_2 from In_2CO. It is reasonably possible to desorb hydrogen from In_2CO by simply exposing it to electric fields without exposing it to any other external media including temperature, pressure, or chemical immersion.

4. Summary

The structural, electronic, charge transfer, adsorption kinetics, and hydrogen storage capacity are calculated for In_2CO using first principles strategies. The bonding interaction between the In_2CO and H_2 molecule is found strong enough for the realization of solid-state hydrogen storage. The desorption temperature, calculated using the average TD for $30H_2$–In_2CO, was found 241 K, with TDH at around 300 K and an H_2 storage capacity of 2.54 wt%. Thermal stability and H_2 desorption from the material were confirmed through AMID simulations at 100 K, 200 K, and 300 K. The desorption temperature derived from the Van't Hoff equation, along with insights from the AMID simulations, highlights a strong correlation, suggesting that In_2CO has potential to efficiently store hydrogen. The electric field desorption of H_2 molecules from the In_2CO surface was also studied which revealed that at 10 V/Å all the entire molecules were successfully desorbed from the surface. The results of this study predict the potential of the In_2CO slab for application in solid-state hydrogen storage.

CRediT authorship contribution statement

Hira Batool: Writing – original draft, Methodology, Formal analysis, Data curation. **Abdul Majid:** Writing – review & editing, Supervision, Resources, Conceptualization. **Iram Shahzadi:** Writing – review & editing, Methodology, Investigation. **Mohammad Alkhedher:** Visualization, Validation, Methodology. **Abdul Manan:** Visualization, Validation, Methodology. **Sajjad Haider:** Visualization, Validation, Methodology. **Kamran Alam:** Visualization, Validation, Methodology.

Ethical approval

Not applicable.

Availability of data and materials

Not applicable.

Declaration of competing interest

The authors declare that they have no known competing financial interests or personal relationships that could have appeared to influence the work reported in this paper.

Acknowledgment

The authors sincerely appreciate funding from Researchers Supporting Project number (RSP2024R399), King Saud University, Riyadh, Saudi Arabia.

References

[1] Wang C, et al. The roles of hydro, nuclear and biomass energy towards carbon neutrality target in China: a policy-based analysis. Energy 2023;262:125303.
[2] Hassan I, et al. Hydrogen storage technologies for stationary and mobile applications: review, analysis and perspectives. Renew Sustain Energy Rev 2021; 149:111311.
[3] Meduri S, Nandanavanam J. Materials for hydrogen storage at room temperature–An overview. Mater Today Proc 2023;72:1–8.
[4] Zheng J, et al. Development of high pressure gaseous hydrogen storage technologies. Int J Hydrogen Energy 2012;37(1):1048–57.

[5] Panigrahi PK, Chandu B, Motapothula MR, Puvvada N. Potential benefits, challenges and perspectives of various methods and materials used for hydrogen storage. Energy Fuels 2024;38(4):2630–53.
[6] Chen X, et al. Ca-decorated borophene as potential candidates for hydrogen storage: a first-principle study. Int J Hydrogen Energy 2017;42(31):20036–45.
[7] Ma L-C, et al. Calcium decoration of boron nitride nanotubes with vacancy defects as potential hydrogen storage materials: a first-principles investigation. Mater Today Commun 2021;26:101985.
[8] Ma L, et al. First-principles study of hydrogen storage on Ca-decorated defective boron nitride nanosheets. Phys E Low-dimens Syst Nanostruct 2021;128:114588.
[9] Ataca C, Aktürk E, Ciraci S. Hydrogen storage of calcium atoms adsorbed on graphene: first-principles plane wave calculations. Phys Rev B 2009;79(4):041406.
[10] Hussain T, et al. Calcium doped graphane as a hydrogen storage material. Appl Phys Lett 2012;100(18).
[11] Anikina E, et al. Elucidating hydrogen storage properties of two-dimensional siligraphene (SiC 8) monolayers upon selected metal decoration. Sustain Energy Fuels 2020;4(11):5578–87.
[12] Hu S, et al. C7N6 monolayer as high capacity and reversible hydrogen storage media: a DFT study. Int J Hydrogen Energy 2021;46(42):21994–2003.
[13] Qiu N-x, et al. A first-principle study of calcium-decorated BC2N sheet doped by boron or carbon for high hydrogen storage. Int J Hydrogen Energy 2014;39(17):9307–20.
[14] Kalwar BA, et al. Enhanced storage capacity of hydrogen based on Li-decorated 2D BC6N under ambient conditions: first-principles study. Comput Mater Sci 2024;231:112621.
[15] Cai Y, et al. Pore modulation of hydrogen-bonded organic frameworks for efficient separation of propylene. Angew Chem 2023;135(37):e202308579.
[16] Xu W-C, et al. Investigation of hydrogen storage capacity of various carbon materials. Int J Hydrogen Energy 2007;32(13):2504–12.
[17] Liu Y, Ren L, He Y, Cheng HP. Titanium-decorated graphene for high-capacity hydrogen storage studied by density functional simulations. J Phys Condens Matter 2010;22(44):445301.
[18] Haldar S, Mukherjee S, Singh CV. Hydrogen storage in Li, Na and Ca decorated and defective borophene: a first principles study. RSC Adv 2018;8(37):20748–57.
[19] Joseph J, et al. Borophene and boron fullerene materials in hydrogen storage: opportunities and challenges. ChemSusChem 2020;13(15):3754–65.
[20] Zhang X, Tang C, Jiang Q. Electric field induced enhancement of hydrogen storage capacity for Li atom decorated graphene with Stone-Wales defects. Int J Hydrogen Energy 2016;41(25):10776–85.
[21] Liu Y, et al. A DFT study on enhanced adsorption of H2 on Be-decorated porous graphene nanosheet and the effects of applied electrical fields. Int J Hydrogen Energy 2021;46(7):5891–903.
[22] Sathishkumar N, Wu SY, Chen HT. Boron-and nitrogen-doped penta-graphene as a promising material for hydrogen storage: a computational study. Int J Energy Res 2019;43(9):4867–78.
[23] Ariharan A, Viswanathan B, Nandhakumar V. Nitrogen doped graphene as potential material for hydrogen storage. Graphene 2017;6(2):41–60.
[24] Kayanuma M, Ikeshoji T, Ogawa H. Theoretical study of hydrogen chemisorption to nitrogen-substituted graphene-like compounds. Bull Chem Soc Jpn 2011;84(1):52–7.
[25] Zhang L, et al. DFT study of superlight ambient temperature reversible H2 storage media based on Li decorated on new planar BCN. Applied Surface 2023;622:156947.
[26] Yuan L, et al. A first principles study of hydrogen storage capacity for Li-decorated porous BNC monolayer. Computational and Theoretical Chemistry 2022;1208:113578.
[27] Wang YS, et al. Metal decorated monolayer BC2N for hydrogen storage. Computational materials science 2012;60:181–5.
[28] Rahimi R, Solimannejad M. Li-decorated Al2C monolayer as a potential template for hydrogen storage: a first-principles perspective. Int J Quant Chem 2021;121(6):e26528.
[29] Rahimi R, Solimannejad M. Hydrogen storage on pristine and Li-decorated BC6N monolayer from first-principles insights. Mol Phys 2021;119(5):e1827177.
[30] Rahimi R, Solimannejad M. Empowering hydrogen storage performance of B4C3 monolayer through decoration with lithium: a DFT study. Surface Interfac 2022;29:101723.
[31] Batool H, Majid A, Manan A, Ahmed N, Haider S, Alam K. First principles investigations on structural, electronic, optical, and thermodynamical properties of bulk and surfaces of In2CO. Materials Science in Semiconductor Processing 2025;186:109092.
[32] Shehbaz A, Majid A, Batool H, Alkhedher M, Haider S, Alam K. Probing the potential of Al2CO/SiC heterostructures for visible light-driven photocatalytic water splitting using first-principles strategies. Journal of Materials Chemistry A 2024;12(21):12657–71.
[33] Majid A, Raza NZ, Ahmad S. Electrochemical performance of P4Se3 as high-capacity anode materials for monovalent and multivalent ion batteries. Materials Chemistry and 2024:129515.
[34] Majid A, Ramzan M, Ahmad S. Unraveling the potential of Al2CO bilayer as anode material in magnesium ion battery and unsuitability for lithium ion battery. Journal of Alloys and Compounds 2024;981:173697.
[35] Batool H, Majid A, Ahmad S, Mubeen A, Alkhedher M, Saeed WS, Al-Owais AA, Afzal A. Phase-dependent properties of manganese oxides and applications in electrovoltaics. ACS Omega 2024;9(2):2457–67.
[36] Seppälä A, Puhakka E, Olin M. Effect of layer charge on the crystalline swelling of Na+, K+ and Ca2+ montmorillonites: DFT and molecular dynamics studies. Clay Miner 2016;51(2):197–211.
[37] Anikina E, et al. Li-decorated carbyne for hydrogen storage: charge induced polarization and van't Hoff hydrogen desorption temperature. Sustain Energy Fuels 2020;4(2):691–9.
[38] Sheng Z, et al. A first-principles study of hydrogen storage capacity based on Li–Na-decorated silicene. Phys Chem Chem Phys 2018;20(20):13903–8.
[39] Ji Y, Dong H, Li YJC. Theoretical predictions on Li–decorated borophenes as promising hydrogen storage materials. ChemistrySelect 2017;2(31):10304–9.
[40] Yu Z, et al. Enhanced hydrogen storage by using lithium decoration on phosphorene. J Appl Phys 2016;120(2).
[41] Haynes WM. CRC handbook of chemistry and physics. CRC press; 2016.
[42] Batool H, et al. A DFT study of quantum electronic transport properties of InTeCl. Mater Sci Semicond Process 2023;168:107842.
[43] Azmat M, et al. A first-principles study on two-dimensional tetragonal samarium nitride as a novel photocatalyst for hydrogen production International Journal of Hydrogen Energy 2023;48(79):30732–40.
[44] Andritsos E, et al. The heat capacity of matter beyond the Dulong–Petit value. J Phys Condens Matter 2013;25(23):235401.
[45] Yang X, et al. Two-dimensional aluminum phosphide semiconductor with tunable direct band gap for nanoelectric applications. RSC Adv 2020;10(42):25170–6.
[46] Majid A, Najam U, Ahmad S. On the prospects of using B4C3 as a potential electrode material for lithium-ion batteries. Mater Sci Semicond Process 2024;176:108320.
[47] Majid A, Khadim B, Alkhedher M, Haider S, Akhtar MS. Modeling of inert gas sensors using first principles methods. IEEE Sensor J. 2023;23(16):18118–24.
[48] Mao SS, Shen S, Guo L. Nanomaterials for renewable hydrogen production, storage and utilization. Prog Nat Sci: Mater Int 2012;22(6):522–34.
[49] Van de Walle CG, Neugebauer J. Hydrogen in semiconductors. Annu Rev Mater Res 2006;36(1):179–98.
[50] Bader RFW, Matta CF. Atomic charges are measurable quantum expectation values: a rebuttal of criticisms of QTAIM charges. J Phys Chem 2004;108(40):8385–94.
[51] Bultinck P, et al. Atomic charges and the electrostatic potential are Ill-Defined in Degenerate Ground states. J Chem Theor Comput 2013;9(11):4779–88.
[52] Bultinck P, et al. Critical analysis and extension of the Hirshfeld atoms in molecules. J Chem Phys 2007;126(14):144111.
[53] Nikolova V, et al. Atomic charges in describing properties of aromatic molecules. J Org Chem 2019;84(4):1908–15.
[54] Zhang S, et al. Three-dimensional metallic boron nitride. J Am Chem Soc 2013;135(48):18216–21.
[55] Savin A, et al. ELF: the electron localization function. Angew Chem Int Ed Engl 1997;36(17):1808–32.
[56] Bratsch SG. A group electronegativity method with Pauling units. J Chem Educ 1985;62(2):101.
[57] Cordero B, et al. Covalent radii revisited. Dalton Trans 2008;(21):2832–8.
[58] Shannon Rt, Prewitt C. Revised values of effective ionic radii. Acta Crystallogr B Struct Crystallogr Cryst Chem 1970;26(7):1046–8.
[59] Ströbel R, et al. Hydrogen adsorption on carbon materials. J Power Sources 1999;84(2):221–4.
[60] Mounssef JrB, et al. DFT study of H 2 adsorption at a Cu-SSZ-13 zeolite: a cluster approach. Physical Chemistry Chemical Physics 2021;23(16):9980–90.
[61] Sun X, et al. Efficient hydrogen storage capacity of La3B18: a DFT study. Int J Hydrogen Energy 2023;48(21):7807–13.
[62] Thomas KM. Hydrogen adsorption and storage on porous materials. Catal Today 2007;120(3–4):389–98.
[63] Panella B, Hirscher M, Roth S. Hydrogen adsorption in different carbon nanostructures. Carbon 2005;43(10):2209–14.
[64] Arellano LG, et al. Hydrogen storage on tin carbide monolayers with transition metal adatoms. Int J Hydrogen Energy 2023;48(96):37500–9.
[65] Ming-Wen Z, et al. Tunable adsorption and desorption of hydrogen atoms on single-walled carbon nanotubes. Chin Phys Lett 2002;19(10):1498.
[66] Zhou J, et al. Electric field enhanced hydrogen storage on polarizable materials substrates. Proc Natl Acad Sci USA 2010;107(7):2801–6.